Nanoscale

Accepted Manuscript

This article can be cited before page numbers have been issued, to do this please use: P. Gupta, B. Singh, K. Roy, A. Sarkar, M. Waschk, T. Brückel and S. Bedanta, *Nanoscale*, 2021, DOI: 10.1039/D0NR06228F.

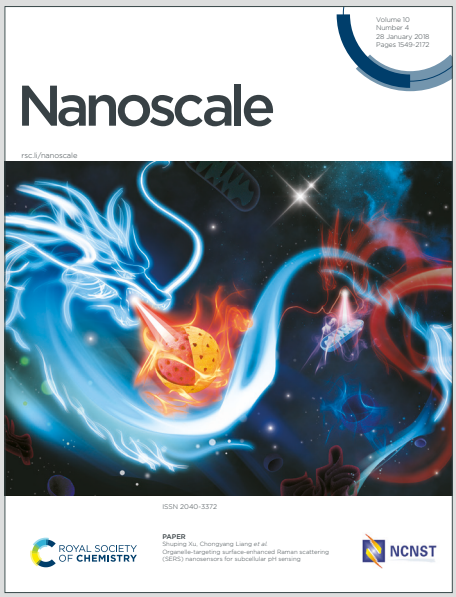

ROYAL SOCIETY OF CHEMISTRY

rsc.li/nanoscale

View Article Online
DOI: 10.1039/D0NR06228F

ARTICLE TYPE

Cite this: DOI: 00.0000/xxxxxxxxxx

Simultaneous observation of anti-damping and inverse spin Hall effect in $La_{0.67}Sr_{0.33}MnO_3$/Pt bilayer system†

Pushpendra Gupta,[a] Braj Bhusan Singh,[a] Koustuv Roy,[a] Anirban Sarkar,[b] Markus Waschk,[b] Thomas Brueckel,[b] and Subhankar Bedanta[a]

Received Date
Accepted Date

DOI: 00.0000/xxxxxxxxxx

Manganites have shown potential in spintronics because they exhibit high spin polarization. Here, by ferromagnetic resonance we have studied the damping properties of $La_{0.67}Sr_{0.33}MnO_3$/Pt bilayers which are prepared by oxide molecular beam epitaxy. The damping coefficient (α) of $La_{0.67}Sr_{0.33}MnO_3$ (LSMO) single layer is found to be 0.0104. However the LSMO/Pt bilayers exhibit decrease in α with increase in Pt thickness. This decrease in the value of α is probably due to high anti-damping like torque. Further, we have investigated the angle dependent inverse spin Hall effect (ISHE) to quantify the spin pumping voltage from other spin rectification effects such as anomalous Hall effect and anisotropic magnetoresistance. We have observed a high spin pumping voltage ($\sim 20\ \mu V$). The results indicate that both anti-damping and spin pumping phenomena are occurring simultaneously.

1 Introduction

Spintronics devices have demonstrated high data storage capacity and miniaturization of computer logics. For the development of next generation devices low power and high speed are the key requisites. Pure spin current (J_s) based devices have shown potentials for fulfilling these requirements due to minimal involvement of charge current (J_c). In this context, ferromagnetic (FM)/heavy metal (HM) hetrostructures are model systems to investigate various spin dependent phenomenon [1–4].

Generation of pure spin current has been demonstrated by ferromagnetic resonance (FMR) through spin pumping mechanism [5–8]. This pure spin current can lose their spin angular momentum in the presence of high spin orbit coupling (SOC) in HM materials e.g Pt, W, Ta etc. The loss of spin angular momentum can develop a voltage by asymmetric scattering of spin, which is known as inverse spin Hall effect (ISHE) [9,10]. SOC is an important factor for observation of large ISHE. Because of the spin-orbit interaction, different spins (up and down) move in one direction and hence an electric field is developed transverse to the movement of spins [11–13]. In ISHE process J_s is converted to J_c and these two physical parameters are related by the below equation:

$$\mathbf{J_c} = \theta_{\mathbf{SH}}\, \mathbf{J_s} \times \sigma \qquad (1)$$

where θ_{SH} is the spin Hall angle (SHA) and σ is the spin polarization vector transverse to the direction of J_s. The value of SHA, therefore, defines the charge to spin current conversion efficiency. The absorption of spin current (J_s^{abs}) generated by HM into FM create a spin transfer torque, which can be quantified by spin orbit torque (SOT) efficiency $\xi_{SH} = (2e/\hbar)J_s^{abs}/J_c$ [14]. It is noted here that in such FM/HM heterostructures, spin pumping increases the value of Gilbert damping coefficient (α) due to absorption of spin angular momentum in HM layer [15,16]. Further in such FM/HM bilayers another type of torque may occur which is called as anti-damping torque [17,18]. This later torque will lead to a decrease in damping value of the bilayer as compared to the reference single FM layer. It is known that a large value of ξ_{SH} and lower α are the important parameters for the development of power efficient devices. Therefore the anti-damping torque may help in achieving magnetization switching at lower current density which is proportional to α/ξ_{SH}, where α is the damping constant of FM/HM bilayer [14]. We note that keeping low α value with spin pumping is a challenge. However anti-damping like torque may help to balance the damping like torque which is opposite of that and hence reduce the value of α in FM/HM heterostructures. Pt has been used widely due to its high conductivity and SHA values. Studies so far are concentrated mostly on Pt and ferromagnetic metals [11,19–21]. In this context insulating ferromagnetic oxides in particular manganites are worth to be investigated for spin to charge conversion based applications. $La_{0.67}Sr_{0.33}MnO_3$ (LSMO) is one

[a] Laboratory for Nanomagnetism and Magnetic Materials (LNMM), School of Physical Sciences, National Institute of Science Education and Research (NISER), HBNI, P.O.-Bhimpur Padanpur, Via –Jatni, 752050, India; E-mail: sbedanta@niser.ac.in
[b] Forschungszentrum Jülich GmbH, Jülich Centre for Neutron Science (JCNS-2) and Peter Grünberg Institut (PGI-4), JARA-FIT, 52425 Jülich, Germany.

† Electronic Supplementary Information (ESI) available: [details of any supplementary information available should be included here]. See DOI: 10.1039/cXCP00000x/

View Article Online
DOI: 10.1039/D0NR06228F

such ferromagnetic oxide which is well known for exhibiting high Curie temperature ($T_C \sim 350$ K) and nearly 100% spin polarization (in bulk)[22]. There are a few reports where spin pumping has been investigated in LSMO/Pt bilayers for which the LSMO is primarily prepared by pulsed laser deposition technique[23–29]. In this work, we aim to study LSMO/Pt bilayers where the samples have been fabricated by oxide molecular beam epitaxy (OMBE) technique. In recent years OMBE has been proven to be an excellent technique to grow high quality complex oxide thin films. Here we show that our LSMO/Pt films are highly resistive. Further we have observed high spin pumping voltage. Both these factors have led to a θ_{SHA} of 0.033. We have also observed decrease in the value of α with increase in spin pumping voltage, which make them very useful for spintronics devices.

2 Experimental Methods

LSMO(t_{LSMO} = 20 nm)/Pt(t_{Pt}) bilayer samples have been prepared on single crystalline $SrTiO_3$(001) substrate using an oxygen plasma assisted molecular beam epitaxy (MBE) system. Samples are named as S1, S2 and S3 for the thickness of Pt (t_{Pt}) = 0, 3 and 10 nm, respectively. Surface and crystalline quality of LSMO films were characterized by *in situ* low energy electron diffraction (LEED) and high energy electron diffraction (RHEED). X-ray diffraction was performed to determine the crystalline phases. Film thicknesses were obtained using X-ray reflectivity. Magnetization dynamics was studied using co-planer wave-guide (CPW) based ferromagnetic resonance (FMR) spectroscopy. Sample was kept on top of CPW in a flip-chip manner[30] as shown in Fig.1(a). To avoid shunting a 25 μm polymer tape was used between sample and CPW. A DC magnetic field H, perpendicular to radio frequency field (h_{rf}), was applied using an electromagnet. α was extracted by measuring FMR spectra in a frequency (f) range of 3-16 GHz with an interval of 0.5 GHz. In this work all FMR and ISHE measurements have been performed at 25 mW microwave power except in the Figure 6 which is a power dependent study in the range 3 to 125 mW. The values of resonance field (H_{res}) and linewidth (ΔH) have been obtained from the Lorentzian fit of the FMR spectra, while the α has been evaluated by fitting the ΔH vs f data. ISHE voltage was measured by a nanovoltmeter. Detailed description of the instrument is described in our previous work [30–33]. The measurements were performed on samples of dimension $\sim 3\times2$ mm^2. Copper wires were used to make contacts using silver paste at the edges of the samples. Angle dependent ISHE has been performed at f = 7 GHz, to disentangle spin rectification effects. Microwave power dependent ISHE measurement has been performed using rf signal generator(SMB–100 model from ROHDE & SCHWARZ).

3 RESULTS AND DISCUSSION

Figure 1(b) and (c) show the LEED and RHEED images for the 20 nm thick LSMO film (sample S1), respectively. The presence of sharp spots (Fig. 1(b)) and streaks (Fig. 1(c)) confirms epitaxial growth of LSMO films on the $SrTiO_3$(001) substrate. The RHEED image also indicate a smooth surface of the LSMO film. These were also confirmed by the x-ray diffraction (data shown in Figure S1 in supplementary information).

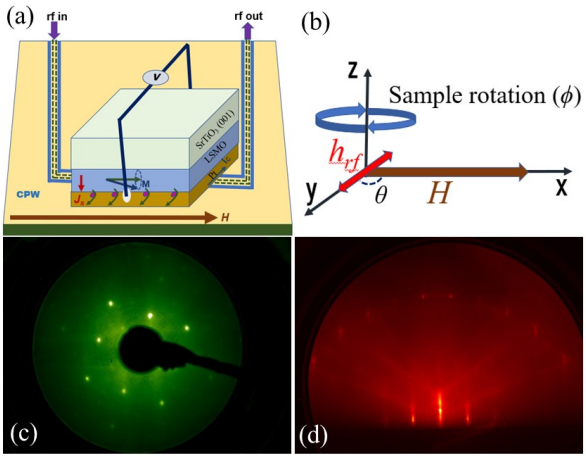

Fig. 1 (a) Experimental setup for FMR and ISHE measurements. (b) The definition of angles and fields (c) LEED (d) RHEED images for sample S1.

In Figure 2 (a), (b) and (c) FMR signal have been shown for samples S1, S2 and S3 respectively. We have plotted FMR signal for different frequencies for all these samples. These FMR signal fitted using the Lorentzian function to get ΔH and H_{res} values for each FMR plot. Figure 3(a) show the f vs H_{res} plot for all the samples obtained from the frequency dependent FMR spectra. The data shown in Figure 3(a) have been fitted by Kittle equation[34],

$$f = \frac{\gamma}{2\pi}\sqrt{(H_{res}+H_K)(H_{res}+4\pi M_{eff}+H_K)} \quad (2)$$

where $\gamma(=\frac{g\mu_B}{\hbar})$, g, μ_B and H_K are gyromagnetic ratio, Lande g–factor, Bohr magneton and in-plane anisotropic field. $4\pi M_{eff}$ $(=4\pi M_S + \frac{2K_S}{M_S t_{FM}})$ is effective demagnetizing field. K_S, M_S and t_{FM} are perpendicular surface anisotropy constant, saturation magnetization and thickness of the LSMO layer, respectively. Further α was evaluated by fitting data of Fig. 3(b) using the relation

$$\Delta H = \Delta H_0 + \frac{4\pi\alpha f}{\gamma} \quad (3)$$

The values of α for samples S1, S2 and S3 are extracted to be 0.0104±0.0003, 0.0046±0.0004 and 0.0037±0.0004, respectively. It should be noted that Pt is a well known metal for exhibiting high SOC and when coupled to a FM layer it may lead to an increase in α. However in our case it is observed that there is a decrease in α with increase in t_{Pt} in comparison to the single LSMO layer (S1). We have plotted t_{Pt} vs α graph (data shown in Figure S2 in supplementary section). It should be noted that all our samples i.e. reference LSMO layer and LSMO/Pt bilayers have been prepared in the same OMBE system. So the change in α in the bilayers as compared to the reference single layer sample clearly indicates that there is an anti-damping. In future growth conditions may be tuned to achieve lower α in the single LSMO film. This may lead to even further reduction in α in the LSMO/Pt bilayers prepared in the same OMBE technique. The reason for this lowering of α could be an anti-damping like torque.

View Article Online
DOI: 10.1039/D0NR06228F

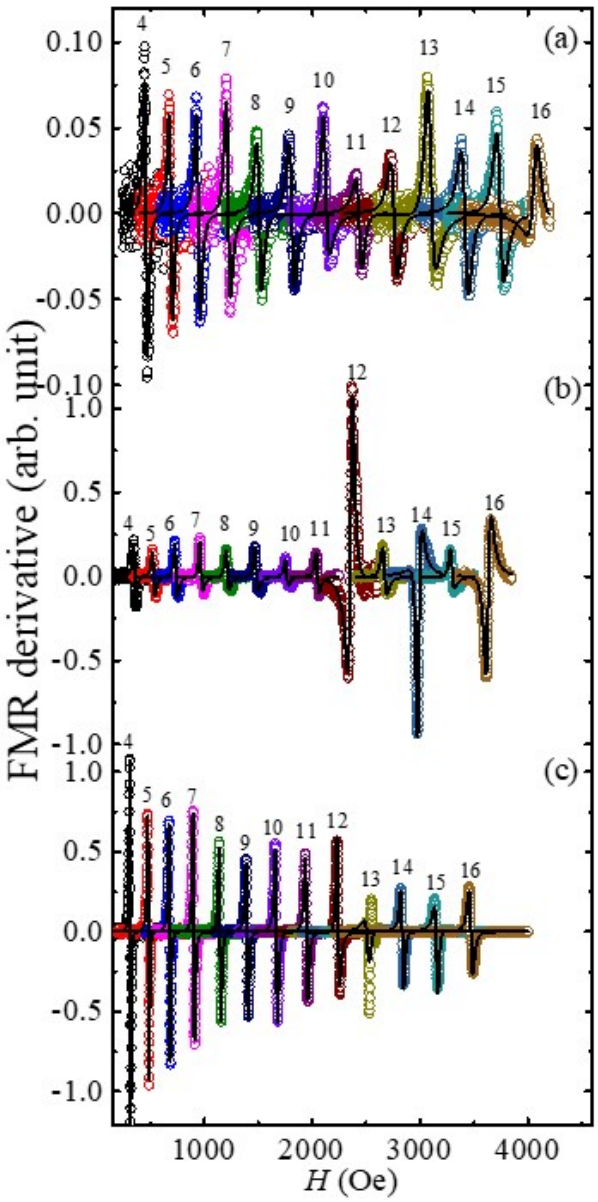

Fig. 2 (a) FMR signal for different frequencies for sample (a) S1, (b) S2 and (c) S3.

Similar anti-damping behavior has been observed in β-Ta and Py bilayer system studied by Behera *et. al.*[35]. The anti-damping in a FM/HM heterostructure can be explained in the following manner. In case of spin flip parameter (ε)<0.1, spin angular momentum at the FM/HM interface creates a non-equilibrium spin density in the Pt layer[36]. This results a back flow of spin current (J_s^0) into the LSMO layer which has two components, (i) parallel, and (ii) perpendicular to instantaneous magnetization $m(t)$ of LSMO layer. The parallel component to $m(t)$ counteracts the spin pumping from LSMO layer and suppresses the spin pumping in Pt layer. Component which is transverse to J_s^0 generates an additional SOT on this in-plane $m(t)$ of LSMO layer. This SOT can be effective up to a distance twice of the spin diffusion length (λ_{SD})[37].

Spin accumulation at the interface is very sensitive to λ_{SD} of Pt

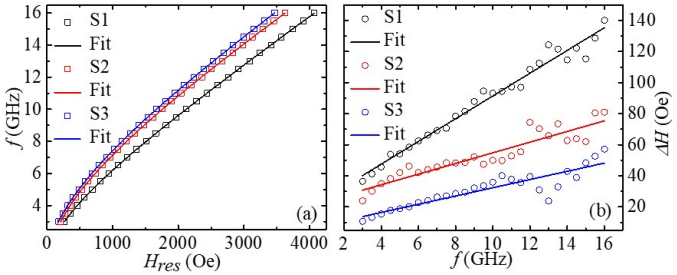

Fig. 3 (a) f vs H_{res} and (b) ΔH vs f for samples S1, S2 and S3.

layer. For $t_{Pt} < \lambda_{SD}$, spin accumulation dominates over the bulk SOC of Pt. This leads to an increase in J_s^0, and a decrease of α. For $t_{Pt} > 2\lambda_{SD}$, J_s^0 decreases which results in a decrease of SOT. This decrease in SOT may lead to an increase in α. We have considered $\lambda_{SD} \sim 5.9$ nm from literature, where the samples studied had similar type of structure[23]. Therefore, it can be concluded that anti-damping like torque is very high and opposite in our samples to overcome damping like torque, which leads to the reduction of the value of α. In a future work samples with Pt thickness more than 12 nm ($2\lambda_{SD}$) will be studied in order to elucidate the antidamping contributions.

In order to quantify the spin pumping we have performed ISHE measurements. Figure 4(a) and (b) represent the ISHE voltage (V_{meas}) vs H for samples S2 and S3, respectively. It is noted that no ISHE signal has been observed for the reference sample S1. We have separated symmetric (V_{sym}) and anti-symmetric (V_{asym}) voltage signal by using the following equation[38],

$$V_{total} = V_{sym}\frac{(\Delta H)^2}{(H-H_{res})^2+(\Delta H)^2} + V_{asym}\frac{(\Delta H)(H-H_{res})}{(H-H_{res})^2+(\Delta H)^2}. \quad (4)$$

Fig. 4(a) and 4(b) show that V_{sym} component is large in comparison to V_{asym}. It is well known that V_{sym} signal originates predominantly from the spin pumping while V_{asym} signal is due to other rectification effects[38].

To separate the rectification effects of anomalous Hall effect (AHE) and anisotropic magneto resistance (AMR) from spin pumping we have performed angle (ϕ) dependent ISHE measure-

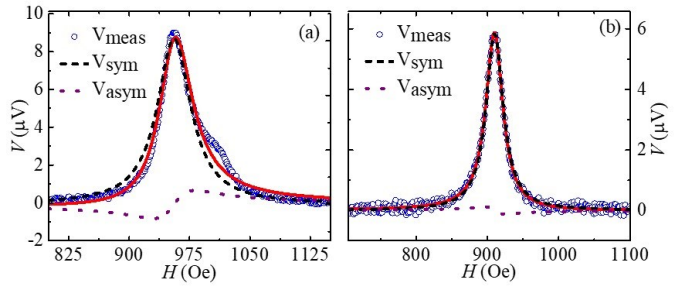

Fig. 4 ISHE voltage for samples S2 and S3 are shown in (a) and (b), respectively. Open circles (in blue) is the measured ISHE voltage and solid line (in red) represents the best fit of the data fitted by equation (4). Dash (in black) and dot (purple) lines represent the V_{sym} and V_{asym} components, respectively, evaluated by fitting to equation (4).

View Article Online
DOI: 10.1039/D0NR06228F

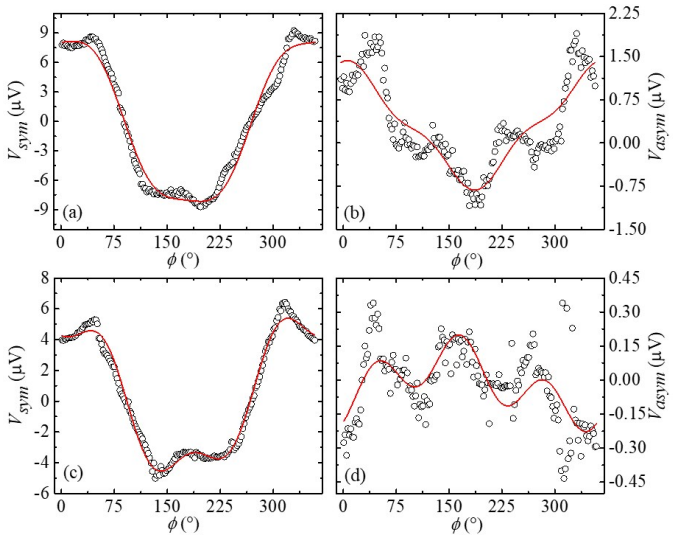

Fig. 5 (a) and (c) Angle dependent V_{sym} for samples S2 and S3, (b) and (d)angle dependent V_{asym} for samples S2 and S3. Figure (a) and (c) were fitted by using equation (5) while figure (b) and (d) were fitted by using equation (6).

ments at a step of 2^0 in the range of 0 to 360^0. Here ϕ is defined as the angle between direction of H and the contacts for voltage measurement. Figure 5(a) and (b) show the angle dependent V_{sym} and V_{asym} for sample S2, respectively. Similarly, Fig. 5(c) and (d) show the evaluated V_{sym} and V_{asym} for the sample S3 respectively. These plots were fitted using the following relations[39],

$$V_{sym} = V_{sp}\, cos^3\phi + V_{AHE}\, cos\phi\, cos\theta + V_{sym}^{AMR\perp}\, cos(2\phi) cos\phi + V_{sym}^{AMR\parallel} \sin(2\phi)\, cos\phi \quad (5)$$

$$V_{asym} = V_{AHE}\, cos\phi\, sin\theta + V_{asym}^{AMR\perp}\, cos(2\phi)\, cos\phi + V_{asym}^{AMR\parallel}\, sin(2\phi)\, cos\phi \quad (6)$$

where V_{sp}, V_{AHE} are voltages due to spin pumping and anomalous Hall effect. Further $V_{asym,sym}^{AMR\parallel}$ and $V_{asym,sym}^{AMR\perp}$ are the parallel and perpendicular components of the AMR voltage, respectively. θ is the angle between h_{rf} and H which is 90° in our case as shown in Figure 1(a). So the equations (5) and (6) can be written as

$$V_{sym} = V_{sp}\, cos^3\phi + V_{sym}^{AMR\perp}\, cos(2\phi)\, cos\phi + V_{sym}^{AMR\parallel} sin(2\phi)\, cos\phi \quad (7)$$

$$V_{asym} = V_{AHE}\, cos\phi + V_{asym}^{AMR\perp} cos(2\phi)\, cos\phi + V_{asym}^{AMR\parallel} sin(2\phi)\, cos\phi \quad (8)$$

$V_{AMR}^{\perp,\parallel}$ can be evaluated by the following equation [39]

$$V_{AMR}^{\perp,\parallel} = \sqrt{(V_{asym}^{AMR\perp,\parallel})^2 + (V_{sym}^{AMR\perp,\parallel})^2} \quad (9)$$

The values V_{sp}, V_{AHE}, $V_{AMR}^{\perp}$ and $V_{AMR}^{\parallel}$ for samples S2 and S3 were obtained from the best fits and listed in table I.

Table 1 Fitted parameters for samples S2 and S3

Sample	$V_{sp}(\mu V)$	$V_{AHE}(\mu V)$	$V_{AMR}^{\perp}(\mu V)$	$V_{AMR}^{\parallel}(\mu V)$
S2	20.05±0.28	0.77±0.05	11.98±0.36	0.34±0.22
S3	12.79±0.11	-0.01±0.01	8.49±0.37	0.55±0.07

From Table I it is observed that V_{sp} decreases for higher Pt thickness. We have calculated θ_{SHA} by using below equation (10) [40,41].

$$V_{ISHE} = \left(\frac{w}{t_{LSMO}/\rho_{LSMO} + t_{Pt}/\rho_{Pt}}\right) \times \theta_{SHA}\lambda_{SD} tanh\left[\frac{t_{Pt}}{2\lambda_{SD}}\right] J_s \quad (10)$$

where J_s is given by,

$$J_s \approx \left(\frac{g_r^{\uparrow\downarrow}\hbar}{8\pi}\right)\left(\frac{\mu_0 h_{rf}\gamma}{\alpha}\right)^2 \times \left[\frac{\mu_0 M_s\gamma + \sqrt{(\mu_0 M_s\gamma)^2 + 16(\pi f)^2}}{(\mu_0 M_s\gamma)^2 + 16(\pi f)^2}\right]\left(\frac{2e}{\hbar}\right) \quad (11)$$

and

$$g_r^{\uparrow\downarrow} = g_{eff}^{\uparrow\downarrow}\left[1 + \frac{g_{eff}^{\uparrow\downarrow}\rho_{Pt}\lambda_{SD}e^2}{2\pi\hbar \tanh\left[\frac{t_{Pt}}{\lambda_{SD}}\right]}\right]^{-1} \quad (12)$$

where w, M_s, and $g_{eff}^{\uparrow\downarrow}$ are the width of CPW, saturation magnetization and spin mixing conductance of the bilayers, respectively. For the evaluation of $g_{eff}^{\uparrow\downarrow}$ the resistivity (ρ) of the samples were calculated by four-probe method. The (ρ) values are 4.79×10^{-5}, 7.33×10^{-7} and 5.25×10^{-7} Ω-m for the samples S1, S2 and S3, respectively. The value of $g_{eff}^{\uparrow\downarrow}$ can be calculated by the following

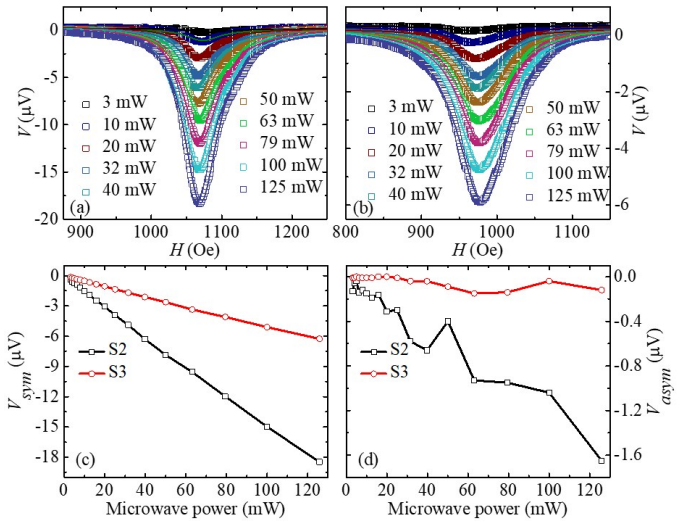

Fig. 6 (a) and (b) Power dependent voltage signal for samples S2 and S3 measured at a f = 7 GHz. (c) and (d) show power dependent V_{sym} and V_{asym} components for samples S2 and S3, respectively.

expression using damping constant[12]:

$$g_{eff}^{\uparrow\downarrow} = \frac{\Delta\alpha 4\pi M_s t_{LSMO}}{g\mu_B} \quad (13)$$

where $\Delta\alpha$ is the change in the α due to spin pumping. The values of θ_{SHA} are evaluated to be 0.033 and 0.014 for samples S2 and

View Article Online
DOI: 10.1039/D0NR06228F

Table 2 Comparison of various parameters from literature for LSMO/Pt bilayers.

Authors	System	Preparation technique	V_{sp} (μV)	$g_{eff}^{\uparrow\downarrow}$ (m^{-2})	Power (mW)	α (10^{-3})
Atsarkin et al.[26]	LSMO(80 nm)/Pt(10 nm)	PLD	0.56	10^{16} - 10^{17}	250	-
Luo et al.[23]	LSMO(20 nm)/Pt(6-30 nm)	PLD	8	1.8×10^{19}	100	4-8
Lee et al.[24]	LSMO(30 nm)/Pt(5-9 nm)	PLD	0.3	2.1×10^{19}	-	1.9 - 2.9
Luo et al.[27]	LSMO(29 nm)/Pt(10nm)	PLD	$\sim$1	-	100	-
Luo et al.[28]	LSMO(20 nm)/Pt(5.5 nm)	PLD	$\sim$5	-	125	$\sim$5.93
Luo et al.[25]	LSMO(26)/Pt(5.5)	PLD	$\sim$3.25	-	40	$\sim$6.50
This work	LSMO(20nm)/Pt(3nm)	OMBE	20.05	1.488×10^{19}	25	4.60

S3, respectively. These θ_{SHA} values matched well to the previously reported values for Pt[42–44] in a similar type of system. For comparison to LSMO/Pt system we have also prepared one sample S4 with structure Si/$Co_{20}Fe_{60}B_{20}$ (5 nm)/Pt (3 nm) sample by DC sputtering system. Detailed analysis has been shown in supplementary information for this sample. The calculated value of θ_{SHA} for sample S4 is 0.022, which is in range of θ_{SHA} for Pt in LSMO/Pt system as mentioned earlier. It is to be noted that V_{sp} for sample S2 is nearly 15 times higher than sample S4, however the enhancement in θ_{SHA} for S2 in comparison to S4 is only 1.1% because SHA is not only dependent of spin pumping voltage but it also depends on many other parameters like thickness of FM, resistivity of the sample, spin mixing conductance etc. Therefore, even spin pumping is quite large for S2, SHA is comparable to S4. In order to control SHA further engineering of sample structure and quality is needed. In order to further confirm that the V_{meas} is primarily due to spin pumping, we have performed microwave power dependent ISHE at 7 GHz. Power dependent measurement was performed in microwave power range of 3 to 125 mW. Microwave power dependent voltage signal is shown in Fig. 6(a) and 6(b) for samples S2 and S3, respectively. Figure 6(c) show the power dependent symmetric part of voltage for samples S2 and S3. The linear increase in microwave power leads to increase in V_{sym} signal strength for both the samples S2 and S3, which confirms that V_{meas} was mainly due to spin pumping. Figure 6(d) shows the V_{asym} dependency over microwave power for samples S2 and S3.

4 Conclusions

We have studied spin pumping and ISHE for LSMO/Pt bilayer samples prepared by oxide molecular beam epitaxy. We have observed a decrease in the value of α with increase in the Pt thickness. This decrease in α value may be due to anti-damping like torque. At the low value of α, we have observed high spin pumping voltage, which makes this system ideal for the development of power efficient spintronics devices. In Table II we show the comparison of various parameters from literature for LSMO/Pt bilayers. We found spin Hall angle value 0.033 for 3 nm Pt thickness which is in range of previously reported values. It seems that the oxide molecular beam epitaxy is a suitable technique to prepare high quality complex oxides. Further study of manganite based system can give the way to control the spin to charge conversion efficiency for the future applications. Attention should also be given to perform spin pumping and/or ISHE experiments on LSMO/Pt samples prepared by PLD where the thickness of Pt should be less than the spin diffusion length i.e. $<$ 5.9 nm. Also the growth conditions and parameters certainly determine the quality of the thin films, interface roughness etc. These parameters have profound effect on the effective damping value of the film. More work is needed to understand in detail about it.

Authors contributions

SB conceived the idea and coordinated the project. The project has been discussed with BBS and TB initially. AS, MW and SB prepared the samples. PG, BBS and KR made the spin pumping and ISHE experiments. The FMR data has been analyzed by PG, BBS and SB. Manuscript is written by PG, BBS and SB. All authors contributed to manuscript corrections.

Conflicts of interest

There are no conflicts to declare.

Acknowledgements

We thank to Department of atomic energy for providing financial support. SB thanks DAAD for providing financial support as a guest scientist to carry out the sample preparation at FZ Juelich, Germany. BBS acknowledges DST for INSPIRE faculty fellowship. PG and KR acknowledge UGC and CSIR for JRF fellowships, respectively.

Notes and references

1 S. Wolf, D. Awschalom, R. Buhrman, J. Daughton, S. Von Molnar, M. Roukes, A. Y. Chtchelkanova and D. Treger, *SCIENCE*, 2001, **294**, 1488–1495.
2 C. Chappert, A. Fert and F. N. Van Dau, *Nat. Mater.*, 2007, **6**, 813–823.
3 I. Žutić, J. Fabian and S. D. Sarma, *Rev Mod Phys.*, 2004, **76**, 323.
4 V. T. Pham, L. Vila, G. Zahnd, A. Marty, W. Savero-Torres, M. Jamet and J.-P. Attaneé, *Nano letters*, 2016, **16**, 6755–6760.
5 O. Mosendz, J. Pearson, F. Fradin, G. Bauer, S. Bader and A. Hoffmann, *Phys. Rev. Lett.*, 2010, **104**, 046601.
6 C. Cerqueira, J. Y. Qin, H. Dang, A. Djeffal, J.-C. Le Breton, M. Hehn, J.-C. Rojas-Sanchez, X. Devaux, S. Suire, S. Migot *et al.*, *Nano letters*, 2018, **19**, 90–99.
7 Y. Tserkovnyak, A. Brataas and G. E. Bauer, *Phys Rev B*, 2002, **66**, 224403.

View Article Online
DOI: 10.1039/D0NR06228F

8 M. Jamali, J. S. Lee, J. S. Jeong, F. Mahfouzi, Y. Lv, Z. Zhao, B. K. Nikolicé, K. A. Mkhoyan, N. Samarth and J.-P. Wang, *Nano letters*, 2015, **15**, 7126–7132.

9 J. Hirsch, *Phys. Rev. Lett.*, 1999, **83**, 1834.

10 S. O. Valenzuela and M. Tinkham, *Nature*, 2006, **442**, 176.

11 T. Kimura, Y. Otani, T. Sato, S. Takahashi and S. Maekawa, *Phys. Rev. Lett.*, 2007, **98**, 156601.

12 E. Saitoh, M. Ueda, H. Miyajima and G. Tatara, *Appl. Phys. Lett.*, 2006, **88**, 182509.

13 A. Takeuchi and G. Tatara, *J. Phys. Soc. Jpn*, 2008, **77**, 074701.

14 M.-H. Nguyen, C.-F. Pai, K. X. Nguyen, D. A. Muller, D. C. Ralph and R. A. Buhrman, *Appl. Phys. Lett.*, 2015, **106**, 222402.

15 K. Ando, S. Takahashi, K. Harii, K. Sasage, J. Ieda, S. Maekawa and E. Saitoh, *Phys. Rev. Lett.*, 2008, **101**, 036601.

16 S. Mizukami, Y. Ando and T. Miyazaki, *Journal of magnetism and magnetic materials*, 2001, **226**, 1640–1642.

17 S. Emori, T. Nan, T. M. Oxholm, C. T. Boone, J. G. Jones, B. M. Howe, G. J. Brown, D. E. Budil and N. X. Sun, *Appl. Phys. Lett.*, 2015, **106**, 022406.

18 N. Behera, A. Kumar, S. Chaudhary and D. K. Pandya, *RSC ADV*, 2017, **7**, 8106–8117.

19 J.-C. Rojas-Sánchez, N. Reyren, P. Laczkowski, W. Savero, J.-P. Attané, C. Deranlot, M. Jamet, J.-M. George, L. Vila and H. Jaffrès, *Phys. Rev. Lett.*, 2014, **112**, 106602.

20 Y. Huo, F. Zeng, C. Zhou and Y. Wu, *AIP Adv.*, 2017, **7**, 056024.

21 X. Zheng, L. Zou, Y. Zhang and J. Cai, *Phys. Rev. Appl.*, 2017, **7**, 044003.

22 J.-H. Park, E. Vescovo, H.-J. Kim, C. Kwon, R. Ramesh and T. Venkatesan, *Nature*, 1998, **392**, 794.

23 G. Luo, J. Lin, W.-C. Chiang and C.-R. Chang, *Sci Rep.*, 2017, **7**, 6612.

24 H. K. Lee, I. Barsukov, A. Swartz, B. Kim, L. Yang, H. Hwang and I. Krivorotov, *AIP Adv.*, 2016, **6**, 055212.

25 G. Luo, C. Chang and J. Lin, *J. Appl. Phys*, 2014, **115**, 17C508.

26 V. Atsarkin, B. Sorokin, I. Borisenko, V. Demidov and G. Ovsyannikov, *J. Phys. D Appl. Phys.*, 2016, **49**, 125003.

27 G. Luo, M. Song, H. Hung, Y. Chiu, J. Kwo, S. Lee, C. Chang and J. Lin, *IEEE Trans. Magn.*, 2012, **48**, 3958 – 3960.

28 G. Luo, M. Belmeguenai, Y. Roussigné, C. Chang, J. Lin and S. Chérif, *AIP Adv.*, 2015, **5**, 097148.

29 I. Benguettat-EL Mokhtari, Y. Roussigné, T. Petrisor Jr, F. Zighem, F. Kail, L. Chahed, V. Pierron, L. Méchin, M. Gabor and M. Belmeguenai, *physica status solidi (b)*, 2020, 2000265.

30 B. B. Singh, S. K. Jena and S. Bedanta, *J. Phys. D Appl. Phys.*, 2017, **50**, 345001.

31 B. B. Singh, S. K. Jena, M. Samanta, K. Biswas, B. Satpati and S. Bedanta, *Phys. Status Solidi Rapid Res. Lett.*, 2019, **13**, 1800492.

32 B. B. Singh and S. Bedanta, *Phys. Rev. Appl.*, 2020, **13**, 044020.

33 S. Nayak, S. Mallick, B. B. Singh and S. Bedanta, *J. Phys. D Appl. Phys.*, 2018, **51**, 055008.

34 C. Kittel, *Phys. Rev.*, 1948, **73**, 155.

35 N. Behera, S. Chaudhary and D. K. Pandya, *Sci. Rep.*, 2016, **6**, 19488.

36 Y. Tserkovnyak, A. Brataas, G. E. Bauer and B. I. Halperin, *Rev. Mod. Phys*, 2005, **77**, 1375.

37 H. Jiao and G. E. Bauer, *Phys. Rev. Lett.*, 2013, **110**, 217602.

38 R. Iguchi and E. Saitoh, *J. Phys. Soc. Jpn*, 2016, **86**, 011003.

39 A. Conca, B. Heinz, M. Schweizer, S. Keller, E. T. Papaioannou and B. Hillebrands, *Phys. Rev. B*, 2017, **95**, 174426.

40 K. Rogdakis, A. Sud, M. Amado, C. Lee, L. McKenzie-Sell, K. Jeon, M. Cubukcu, M. Blamire, J. Robinson, L. Cohen *et al.*, *Phys Rev. Mater.*, 2019, **3**, 014406.

41 K.-R. Jeon, C. Ciccarelli, H. Kurebayashi, J. Wunderlich, L. F. Cohen, S. Komori, J. W. Robinson and M. G. Blamire, *Phys. Rev. Appl.*, 2018, **10**, 014029.

42 Y. Wang, P. Deorani, X. Qiu, J. H. Kwon and H. Yang, *Phys. Rev. Lett.*, 2014, **105**, 152412.

43 X. Tao, Q. Liu, B. Miao, R. Yu, Z. Feng, L. Sun, B. You, J. Du, K. Chen, S. Zhang *et al.*, *SCI ADV.*, 2018, **4**, eaat1670.

44 L. Wang, R. Wesselink, Y. Liu, Z. Yuan, K. Xia and P. J. Kelly, *Phys. Rev. Lett.*, 2016, **116**, 196602.